



HAL
open science

Design of a high order Campbelling mode measurement system using open source hardware

G. De Izarra, Zs. Elter, C. Jammes

► To cite this version:

G. De Izarra, Zs. Elter, C. Jammes. Design of a high order Campbelling mode measurement system using open source hardware. Nuclear Instruments and Methods in Physics Research Section A: Accelerators, Spectrometers, Detectors and Associated Equipment, 2016, 839, pp.12-22. 10.1016/j.nima.2016.09.038 . cea-02388644

HAL Id: cea-02388644

<https://cea.hal.science/cea-02388644>

Submitted on 2 Dec 2019

HAL is a multi-disciplinary open access archive for the deposit and dissemination of scientific research documents, whether they are published or not. The documents may come from teaching and research institutions in France or abroad, or from public or private research centers.

L'archive ouverte pluridisciplinaire **HAL**, est destinée au dépôt et à la diffusion de documents scientifiques de niveau recherche, publiés ou non, émanant des établissements d'enseignement et de recherche français ou étrangers, des laboratoires publics ou privés.

Design of a high order Campbell mode measurement system using open source hardware

G. de Izarra^a, Zs. Elter^{b,c}, C. Jammes^b

^aCEA, DEN,DER, Experimental Programs Laboratory, Cadarache,
F-13108 Saint-Paul-lez-Durance, France

^bCEA, DEN,DER, Instrumentation, Sensors and Dosimetry Laboratory, Cadarache,
F-13108 Saint-Paul-lez-Durance, France

^cChalmers University of Technology, Department of Physics, Division of Subatomic and
Plasma Physics,
SE-412 96 Göteborg, Sweden

Abstract

This paper reviews a new, real-time measurement instrument dedicated for online neutron monitoring in nuclear reactors. The instrument implements the higher order Campbell methods and self-monitoring fission chamber capabilities on an open source development board. The board includes an CPU/FPGA System On a Chip.

The feasibility of the measurement instrument was tested both in laboratory with a signal generator and in the Minerve reactor. It is shown that the instrument provides reliable and robust count rate estimation over a wide reactor power range.

The fission chamber failure detection ability is also verified, the system is able to identify whether the measured count rate change is due to the malfunction of the detector or due to the change of neutron flux. The applied method is based on the change of the frequency dependence of the fission chamber signal power spectral density, due to the malfunction. During the experimental verification, the considered malfunction was the change of the polarization voltage.

Keywords: High order Campbell, FPGA, Measurement system, Count rate estimation

PACS: 29.85.-c, 28.50.Dr, 28.41.Rc

1. Introduction

The recent development of French Sodium-cooled Fast Reactor (SFR) induces the need for new neutron flux monitoring systems in order to enhance the safety features. Given the configuration of the pool type SFR, the neutron instrumentation is planned to be set up in the reactor vessel in order to monitor the neutron flux over a few orders of magnitude [1]. The high temperature fission chambers are the best candidates for this purpose since the typical temperature in the vicinity of the core is around 500 °C [2]. This detector type was extensively studied in the CEA during the nineties and is still under active development. In addition, a research effort is currently done in order to exploit the wide flux range monitoring capability of fission chambers: it was previously shown that the use of high order Campbelling mode (HOC) provides a linear estimation of the neutron flux over a wide range of count rate by suppressing the impact of parasitic noises.

In this framework, a HOC measurement system prototype was developed at the Instrumentation, Sensors and Dosimetry Laboratory (LDCI) of CEA Cadarache. The main goal of the work is to assess the feasibility and the industrial use of such measurement system. To complete the measurement device, a fission chamber malfunction detection module (referred later as "smart-detector" capability) was included.

In this paper, the implementation of HOC method on an open source hardware development board is detailed. First, the general theory of HOC is discussed briefly and the most important advantages of its application are highlighted. The theoretical basis of the fission chamber malfunction detection is also reviewed. Second, the design of the Campbell measurement system is presented: the preference of using a open source hardware with a CPU/FPGA chip at the prototype phase are summarized; The HOC computation algorithm is explained through diagrams and clocking figures; The software dedicated to control the FPGA module is introduced. The last part of the paper is dedicated to the validation of the measurement system through laboratory measurements and in-core experimental campaigns performed at the Minerve reactor.

2. Theoretical background

2.1. High order Campbelling theoretical background

Campbell derived a theorem [3] that links the intensity of a shot noise process consisting of general pulses $f(t)$ with an amplitude distribution to

37 the variance of the process. The generalisation of this theorem was proposed
 38 and its complete derivation has been performed in [4, 5]:

$$s_0 = \frac{\kappa_n}{\langle x^n \rangle \int f^n(t) dt} = \frac{k_n}{C_n}. \quad (1)$$

39 where κ_n is the n th order cumulant of the signal, s_0 is the count rate and
 40 $\langle x^n \rangle$ stands for the n th order raw moment of the amplitude distribution.
 41 Commonly, the methods in which $n \geq 3$ are called higher order methods.
 42 Eq. (1) shows that if the pulse shape and the amplitude distribution are
 43 known (therefore the calibration coefficient C_n is determined), and the cu-
 44 mulant (of any order) of the signal is measured, then the mean count rate
 45 s_0 of the signal can be estimated.

46 In the current work, the estimation of the cumulants is performed by
 47 applying unbiased cumulant estimators, called k-statistics [6]. If the mea-
 48 sured signal consists of N discretely sampled values Y_i , then the third order
 49 cumulant estimator is given as:

$$k_3 = \frac{2S_1^3 - 3NS_1S_2 + N^2S_3}{N(N-1)(N-2)}, \quad (2)$$

50 where S_1, S_2, S_3 are the first, second and third order sums of the data points
 51 defined as:

$$S_n = \sum_{i=1}^N Y_i^n \quad (3)$$

52 The performance of high order Campbelling methods have been intensively
 53 studied in [7]; it was shown that the application of higher order methods
 54 sufficiently suppresses the impact of various noises. The linearity of the
 55 count rate estimation over a wide count rate range (from 10^4 to 10^9 cps)
 56 have been verified both numerically and experimentally. It was highlighted
 57 that the application of higher than third order methods do not bring any
 58 practical advantage and accurate count rate estimation can be achieved with
 59 the third order Campbelling based on signal samples of a few ms.

60 2.2. Smart detector theoretical background

61 Eq. (1) shows that any cumulant of the signal may change not only due
 62 to the change in the count rate, but also due to the change in the mean
 63 pulse shape or in the amplitude distribution. The higher order methods are
 64 particularly sensitive to these changes because of the higher exponents in
 65 Eq. (1). The change of the pulse shape and its amplitude may occur due
 66 to a malfunction, such as the reduction of detector pressure or voltage since

67 these result a change in the electron drift velocity. During the measurement
 68 only the change of the cumulant (therefore the change of the estimated count
 69 rate) will be detected, thus we have to be able to decide whether this change
 70 occurred due to the change of the neutron flux around the detector or due
 71 to the malfunction of the detector.

72 Therefore we have to define a measurable quantity of the fission chamber
 73 signal which is sensitive to the pulse shape change but not to the count rate
 74 change. As a previous study shows [?], the width of the power spectral
 75 density (PSD) of the detector signal satisfies this requirement. In this work
 76 the PSD of a signal $y(t)$ is defined as:

$$PSD(f) = \frac{FT(y)FT^*(y)}{T_m} \quad (4)$$

77 where FT stands for the Fourier transform, and T_m is the measurement time

78 It was shown that by measuring the width of the PSD, one can detect
 79 the change of the pulse shape due to the leakage of the filling gas. The
 80 spectral width was defined as the width at the half maximum of the PSD,
 81 it is usually contained in the 0-20 MHz band, which is an easily accessible
 82 frequency band with the modern instrumentation.

83 3. Design of high order Campbelling measurement system

84 The development of an on-line neutron monitoring system, which makes
 85 use of fission chamber signals and works in higher order Campbell mode,
 86 requires:

- 87 • Capability to convert and process the signal at the output of the avail-
 88 able pre-amplifier (between -10 and 10 V for the typical nuclear instru-
 89 mentation).
- 90 • Real-time computation of the first, second and third order sum of the
 91 signal (see Eq. (3)).
- 92 • High sampling frequency in order to resolve the signal consisting of
 93 pulses with a width of a few tens of nanoseconds.
- 94 • Ability to process a large amount of data in real-time (given that a
 95 time window of a few ms has to be applied for accurate estimations).

96 Since this work aims to develop a prototype system and provide proof of
 97 concept, two additional requirements have to be considered:

- 98 • Versatility in order to modify the prototype easily and test new imple-
99 mentations.
- 100 • Large user community and preferably open source philosophy in order
101 to facilitate the learning and to get fast technical support.

102 3.1. Hardware selection

103 Recently several single board computers and system on a chip (SoC)
104 boards revolutionized and facilitated the development of digital measurement
105 instruments. Based on the above defined criteria, the Red-Pitaya board was
106 chosen; it was created to provide a customizable measurement system with a
107 generous amount of examples according to the open source philosophy. Due
108 to its low footprint, low price and relatively large user community, it fulfills
109 all the requirements which were expected at the prototype stage.

110 The Red-Pitaya board is built around a Xilinx Zync 7010 SoC which
111 embeds an FPGA and a dual core Arm CPU clocked at 668 MHz. The Red-
112 Pitaya board hosts two Analog-to-Digital Converters (ADC) and two Digital-
113 to-Analog Converters (DAC) which are directly connected to the FPGA. The
114 ADCs have a sampling frequency of 125 MHz and a resolution of 14 bits. The
115 board provides two measurement ranges through jumper positions: ± 0.6 V
116 and ± 16 V. The great strength of the FPGA is letting to design a circuit,
117 which allows to process the data in line, therefore reducing the time, and
118 the memory storage for heavy computations. This makes FPGAs ideal to
119 perform simple computing patterns on a vast amount of data in real time.
120 These characteristics fulfill all the above stated requirements to develop an
121 online neutron monitoring system: the board is able to process the signal
122 at output of the most common pre-amplifier (0,10 V for the CEA PADF and
123 -10,0 V for the Canberra ADS pre-amplifiers applied in this work), to resolve
124 the fission chamber pulses (with a length of few tens of ns), and to perform
125 the real-time processing of large amount of data.

126 It has to be mentioned, that although it may seem that the CPU could
127 handle all the data processing needed to calculate the high order sums of the
128 signal, the real time computation with the CPU couldn't be realized due to
129 the huge amount of data transfer and operations (≈ 750 [Mop/s]) it implies.
130 Therefore, in the neutron monitoring instrument, the FPGA was dedicated
131 to the low level, time critical, redundant operations (namely computing the
132 power sums of the signal values), whereas more complicated operations were
133 performed on the CPU.

134 The FPGA of the board is configured using Verilog, a low level Hardware
135 Description Language (HDL), and the softwares running on the CPU are de-
136 veloped in C language. It has to be recognized that development with a

137 hardware description language is more cumbersome than with a normal pro-
138 cedural language (the main constraints are detailed in the following section).
139 Thus, during the design of the instrument the use of the low level computing
140 was kept to a reasonable minimum, in order to facilitate the development and
141 the maintainability of the device while keeping CPU computing power for
142 prospective data processing. The following sections are devoted to explain
143 the inner design of the new measurement system.

144 3.2. Third order cumulant measurement system

145 The most time consuming operations, while computing the third order
146 cumulant estimator k_3 (Eq. 2), are the computations of the sums S_1 , S_2 and
147 S_3 (Eq. 3), since the higher order power of each signal sample is required
148 in real-time. On the other hand, the further operations to compute the
149 estimator k_3 based on the sums, has to be done only once at the end of
150 the measurement time and don't exhibit any simple computational patterns.
151 Consequently, the real-time computation of the sum terms were realized
152 on the FPGA, and, after the transfer of the sums to the CPU, the final
153 operations to compute the cumulant estimator were performed by a control
154 software running on the CPU.

155 The developed FPGA module of the measurement system is composed of
156 five algorithmic blocks. Two blocks are dedicated to read and write data for
157 the Processing System (PS, i.e. the computer part of the SOC). One block
158 is in control of the measurement soft reset. Two blocks are directly related
159 to computation of the third order cumulant estimator terms. The function
160 and the realisation of the last two blocks are detailed below.

161 3.2.1. Unbiased cumulant estimation FPGA module

162 The algorithm design starts with the definition of registers (variables used
163 to store data): s_1 , s_2 and s_3 contain respectively the sum of single, square
164 and cubic power of the samples for N number of samples. It is favorable to
165 limit the number of samples to a power of 2 to simplify division by N into bit
166 shifting operation. It was shown previously that the proper measurement
167 time for the cumulant was between a hundred of micro-seconds and a few
168 tens of millisecond [7], in terms of number of samples, this corresponds to
169 N between 2^{22} (33.5 ms) and 2^{14} (131 μ s) if the sampling frequency is 125
170 MHz; Register N size was set to 23 bits.

171 The sizes of s_1 , s_2 and s_3 have to be carefully defined as well, since their
172 sizes have to be adequately large in order to avoid overflows. The develop-
173 ment board provides two's complement signed 14 bits samples, an addition
174 of two samples has to be stored on 15 bits, where as their multiplication is

175 stored on 28 bits. This implies that `s1`, which contains up to `N` summed data
176 has to be 36 bits wide because of the maximum value of `N`, which is 2^{22} . `s2`
177 and `s3` must be 50 and 64 bits wide in order to contain respectively the sum
178 of square and cubic power of samples.

179 Once each used register has the proper size, the algorithm can be de-
180 signed. Two important constraints have to be taken into account at the low
181 level computing. First, every operation in an algorithmic block is performed
182 in parallel during a clock tick; the results of the operations will be available
183 at the end of the clock tick which prohibits the use of regular procedural
184 programming. However, branching (i.e. conditional tests) does not consume
185 any computation time. Second, only one operand can be used in an opera-
186 tion; it implies to pipeline the computation of square and cubic power over
187 several clock ticks.

188 Fig. 1 summarizes the implemented algorithm: the main algorithmic
189 block contains a loop dedicated to the computation of the sums. To provide a
190 better understanding of the time operation of the algorithm, Fig. 2 illustrates
191 is clocking diagram for $N = 4$.

192 At each clock tick, the data stream coming from the ADC (`adc_a`) is stored
193 into two temporary registers (`single` contains the ADC value and `double`←
194 contains the square of the ADC value), which are used to pipeline the power
195 computation. In the same time, `adc_a` is added to `s1`, `double` to `s2` and `triple`
196 to `s3` (`triple` is also a temporary register dedicated to store the cubic power
197 of samples, it is fed with the result of the multiplication `single*double`).

198 A sample counter (`sample`) is incremented at each cycle to keep track of
199 the amount of samples processed since the start of the current measurement.
200 When `sample` is equal to `N`, the completion process and the transfer of `s1`, `s2`,
201 `s3` to registers accessible by the PS (namely `s1mem`, `s2mem`, `s3mem`) begins. To
202 transfer the sums to the area from which the data transfer towards the CPU
203 takes place, intermediate registers (namely `s1inter`, `s2inter`, `s3inter`) have to
204 be used to store the sums due to the pipelining. The reason is that the final
205 values of `s2` and `s3` will be available respectively one and two clock ticks after
206 `s1`, however, the data transfer has to be done in one clock cycle in order not
207 to mix old and new data in registers where the CPU has access.

208 To achieve the transfer, first the flag `data_transfer` responsible for data
209 transfer from intermediate registers to the memory area accessible by CPUs
210 is set to false. In the same clock tick when the `sample` is equal to N , the
211 flag specifying the availability of `s1` (`s1ready`) is set to true, while the flags
212 indicating the availability of `s2` and `s3` (`s2ready` and `s3ready`) are set to false.

213 In the next clock tick, a test `s1ready==true` allows `s1` to be transferred
214 to the intermediate register `s1inter`, while the computation of `s1` restarts.

215 At the same time, `S2ready` is set to true since `S2` will be ready for the next
216 tick. During the following tick, a test `S2ready==true` allows `S2` to be copied
217 to `S2inter` and its computation restarts, while `S3ready` is also set to true. In
218 the next clock tick, the test `S3ready==true` is verified and the copy of `S3`↔
219 to `S3interm` is performed; a register which keeps track of measurement time
220 (`time_stamp`) is also incremented and the flag `data_transfer` is reset to true↔
221 . All the sums can now be copied from intermediate registers to the ones
222 accessible by the PS (the algorithmic block responsible for this transfer is
223 summarized in Fig.3)), while the registers containing the sums, `S1`, `S2`, `S3` are
224 already filled with the data of the new measurement.

225 3.2.2. Control software of the High Order Campbell module

226 A software was written in a high level programming language to control
227 the FPGA module. Its main task is to read the data provided by the FPGA
228 at the designated memory addresses, to construct the estimator $k3$ and to
229 make it available for further processing. At this phase, two constraints have
230 to be considered to fulfill the requirements of real-time monitoring: first,
231 the software must be capable to construct the estimator in a time window
232 shorter than the duration of the measurement without being slowed down
233 by the post-processing of data. Second, it should not miss any measurement
234 and should store each result produced in the memory for further processing.

235 In order to fulfill these requirements, the software design uses two threads,
236 which allow to take advantage of the dual core architecture. One transfers
237 the available measurement into the memory of the PS: it reads the time
238 stamp computed by the FPGA, and if this time is larger than the one stored
239 in computer memory, $S1$, $S2$ and $S3$ are transferred and $k3$ estimation is
240 constructed. The second thread is responsible for heavy and slow processes
241 such as printing and saving the cumulant estimator. It has only access to
242 the data provided by the measurement thread. In order not to lose data, a
243 FIFO (First In First Out) pile can be used by the measurement thread to
244 store the terms of the cumulant. Both threads are detailed through diagrams
245 available in Fig. 4 and Fig. 5.

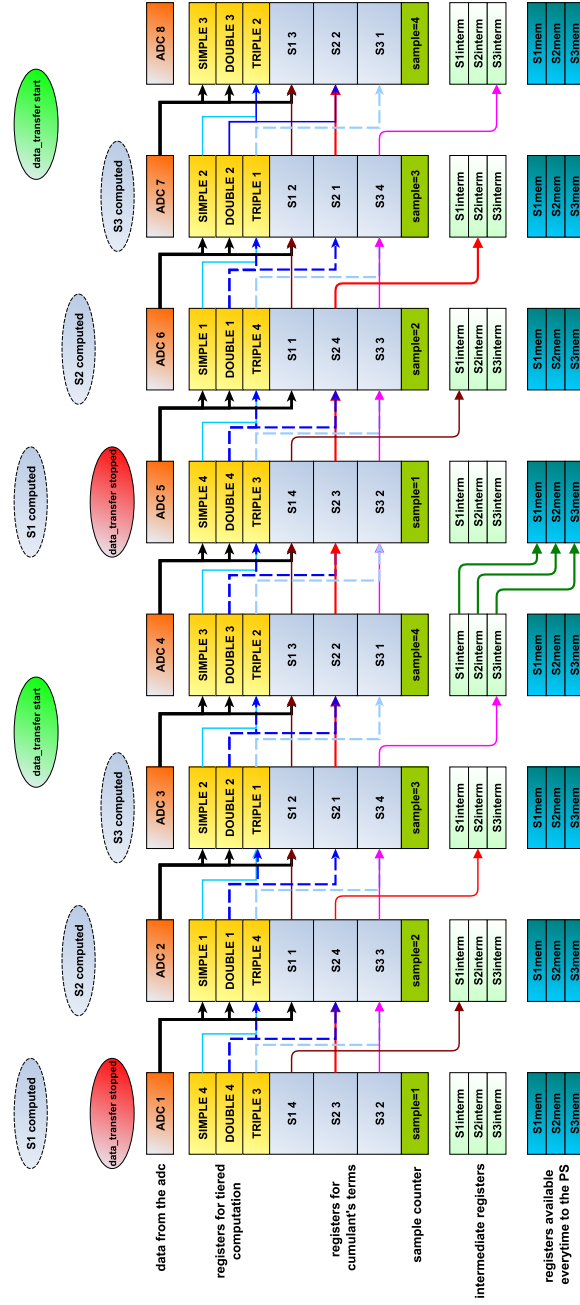


Figure 2: Clocking diagram of the algorithm for computation of the cumulant terms. For the sake of simplicity, the number of samples per measurement is set to $N = 4$. The squares represent the state of registers at each tick while the arrows summarize the operation performed during the tick. Bubbles at the top of the diagram are related to flags for finishing the computation and initiating memory transfer.

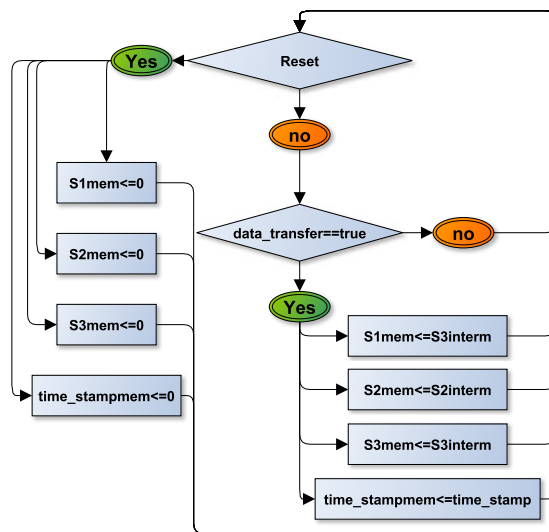


Figure 3: Diagram of the algorithmic block dedicated to transfer data from the computing block to the block in charge of communication between the FPGA and the PS.

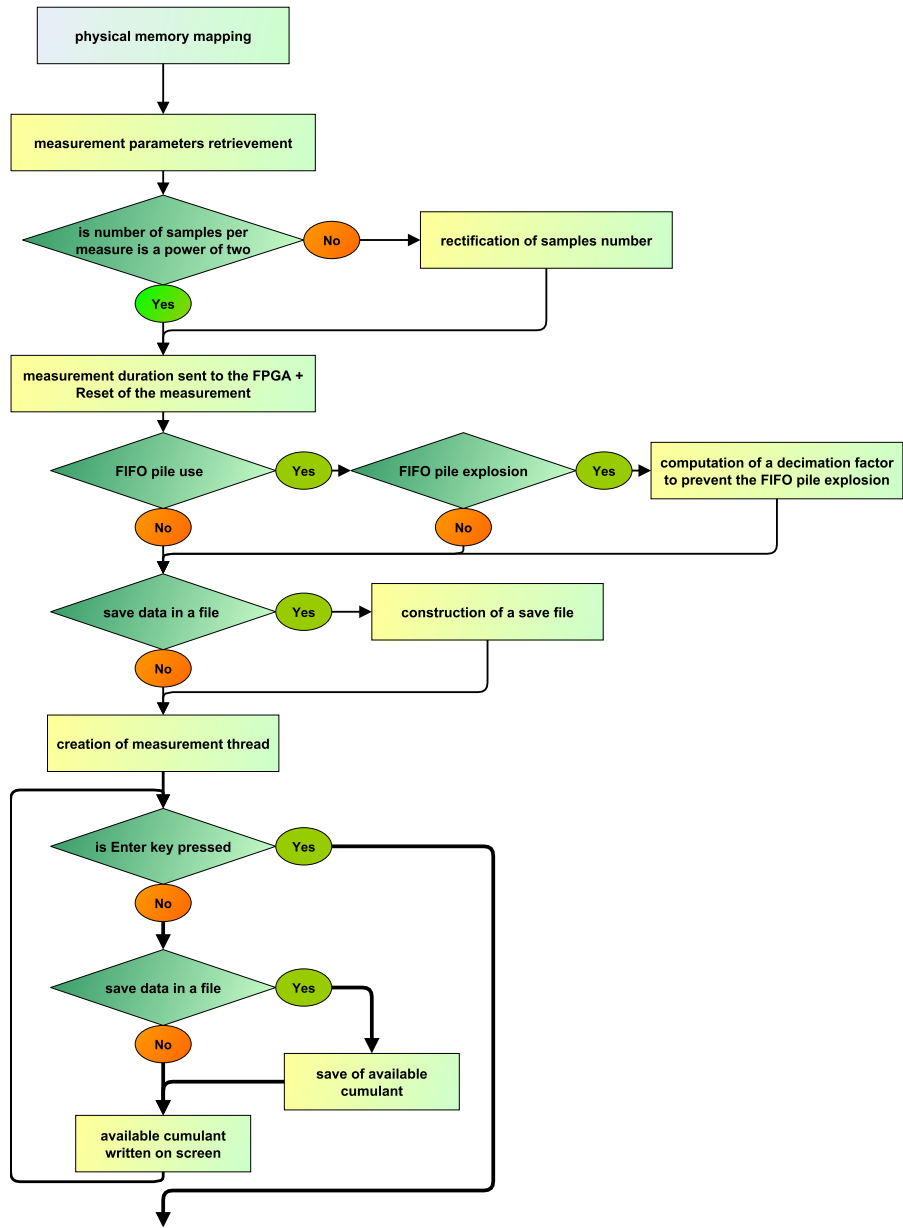


Figure 4: Diagram of the HOC measurement system control software.

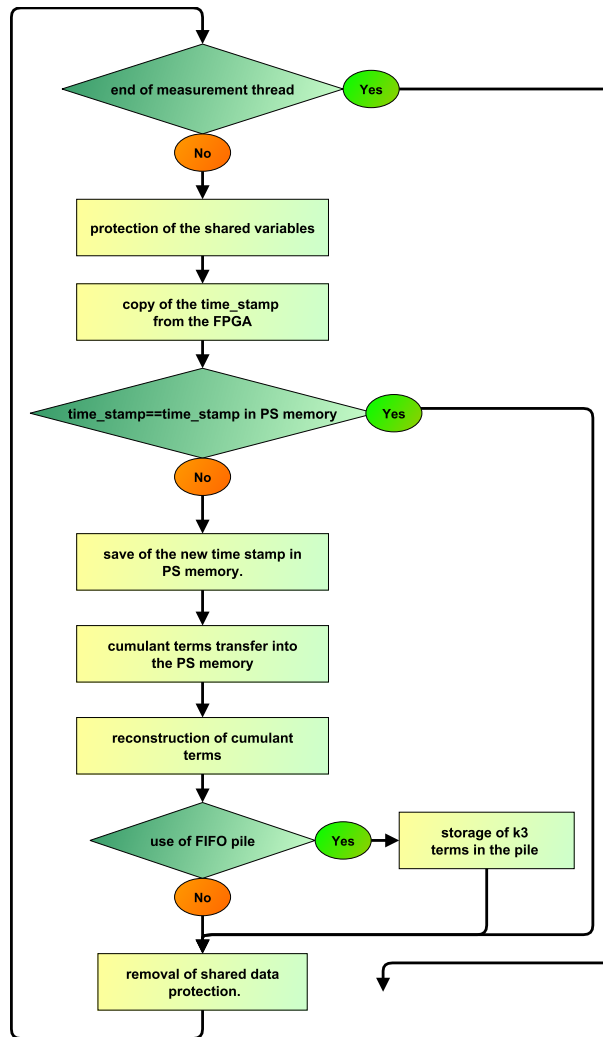


Figure 5: The measurement loop schematized here is called by the measurement thread independently from the main software.

246 *3.3. Smart detector system*

247 The measurement prototype was completed with smart detector capabil-
248 ities in order to detect the change in the width of the power spectral density,
249 which indicates a possible malfunction during operation.

250 As it was shown previously [8], it is satisfactory to monitor the power
251 spectral density on the s time scale. In order to minimize the necessary
252 change in the FPGA modules developed for the higher order cumulant com-
253 putations, in the smart detector module, the FPGA (controlled by the PS)
254 is responsible only for recording the raw data. The complex data processing,
255 such as computing the PSD and determining its width, is done on the CPU
256 with specific C routines from the GSL (GNU Scientific Library) [9].

257 *3.3.1. Smart detector FPGA module*

258 The hardware part of the smart detector module consist of a punctual
259 raw data recorder which makes use of the block RAM available on the FPGA;
260 the Artix-7 have 60 blocks of 36 kB RAM which can have a limited set of
261 configuration [10]: Since the data coming from the ADC are 14 bits wide,
262 only 2^{16} data points (0.524 ms) can be stored in the memory.

263 The FPGA module is constructed from three algorithmic blocks available
264 in Fig. 6: the first one stores ADC data into a memory buffer, while the
265 second and third one deal respectively with data transfer to the PS and with
266 message dispatching through the smart detector module.

267 For the sake of simplicity, it was decided to use the memory transfer
268 algorithm included in the Red-Pitaya project and a serialised architecture
269 to move data buffer from the FPGA to the PS: The PS sends the memory
270 address to be read and the memory transfer code block makes ready the
271 related data (`buff[yraw_read_addr]`) for an eventual read command.

272 Even with a limited signal length and slow memory transfer (≈ 12.5
273 Mdata/s), this architecture is suitable for the fission chamber failure detec-
274 tion. Nevertheless, in the future, it is possible to improve this module: since
275 the granularity of memory transfer is 32 bits, transferring more than one 14
276 bits of useful data in a clock tick could speed up the transfer to the PS by a
277 factor 2.

278 *3.3.2. Control software of the smart detector module*

279 The control software of the campbell measurement system was extended
280 in order to include the smart detector capabilities. The general architecture
281 remains the same: two threads are running on the two cores of the CPU.
282 One is dedicated to the measurement and only does lightweight processing
283 while the other is related to heavy data processing (as shown in Fig.7). A

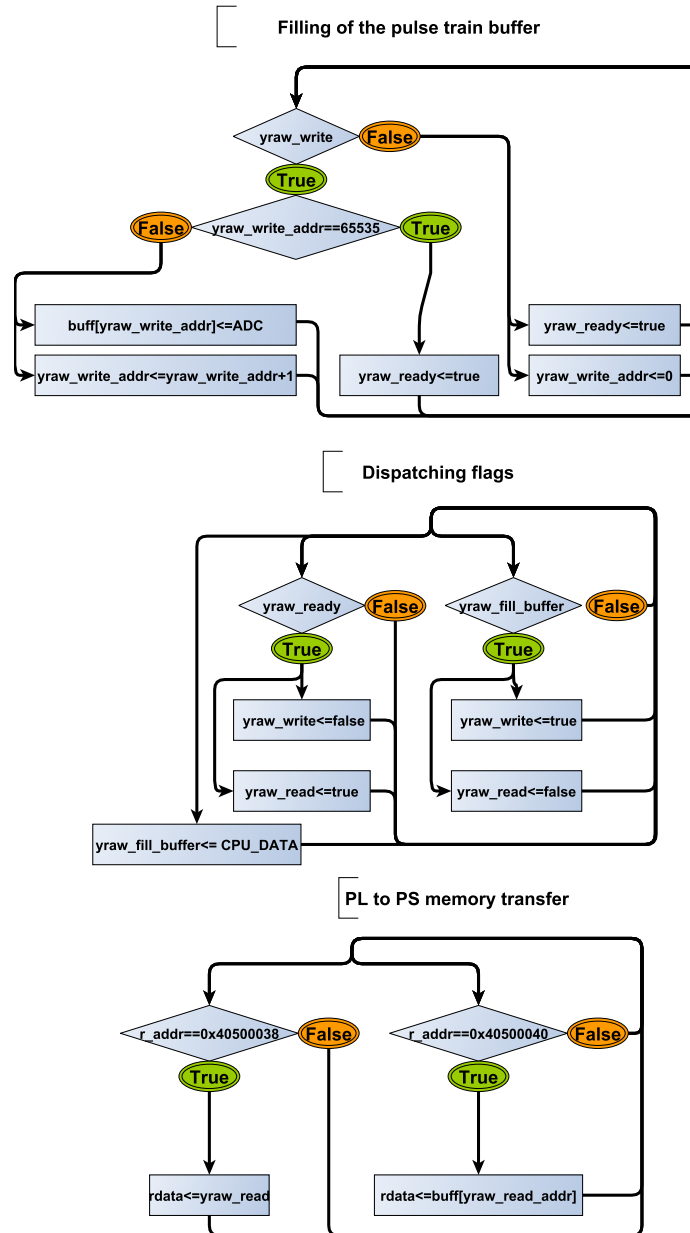


Figure 6: Smart detector algorithm implemented on the FPGA. The register ADC represents a raw sample.

284 flag set by the user at the program start-up (`compute_psd`) allows to enable
285 the smart detector module.

286 The measurement thread was adapted to transfer signal segments: one
287 flag is shared with the data processing thread, `psd_compute_flag` is used to no-
288 tify the FPGA that the signal buffer has to be filled. Then, the measurement
289 thread checks periodically if the data buffer is ready. Once it is ready, the
290 data is transferred. When a complete signal segment has been transferred,
291 the measurement thread indicates it with `psd_compute_flag`.

292 The data processing thread is in charge of PSD computation. When the
293 buffer data is ready to be processed, the thread proceeds to the PSD com-
294 putation after requesting a new signal segment. The spectrum is computed
295 using the Bartlett's method. When the the amount of computed spectra
296 reaches `MAX_PSD`, the average spectrum is computed, and the width of the
297 spectrum is estimated. Finally, the mean spectrum is saved on the disk.

298 4. Experimental validation

299 The measurement system prototype was tested through several experi-
300 ments. During the development phase, experiments in laboratory were per-
301 formed to check whether the FPGA modules are well implemented. Finally,
302 the measurement system was connected to fission chambers and tested in
303 the Minerve reactor under real working conditions. The measurements and
304 the obtained results are detailed in the following sections.

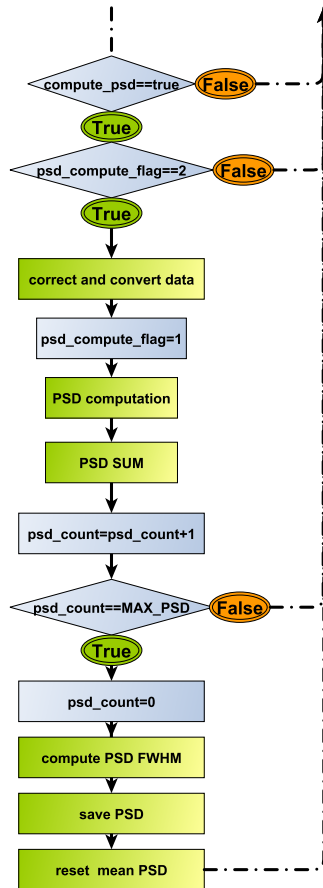
305 4.1. Laboratory validation

306 4.1.1. Validation of the HOC measurement system

307 The validation of the HOC measurement system was done in two steps.
308 In the first step, the proper computation and transfer of S_1 , S_2 and S_3 was
309 checked by replacing the ADC input data by a constant value of 2. It was
310 verified that for N samples, the computed sums S_1 , S_2 and S_3 are equal to
311 $2N$, $4N$ and $8N$ respectively.

312 In the second step, the accuracy of the third order cumulant estimation
313 was tested with Poisson pulse trains simulated by a pulse train generator.
314 The pulse trains consisted of exponential damped pulses with a width of
315 around 100 ns and a random normally distributed amplitude. The count
316 rates were varying between $4 \cdot 10^5$ to $4 \cdot 10^7$ c/s. The pulse trains were
317 loaded (in the proper format) and played by a Tektronix AWG 5012 signal
318 generator. The datasets were 0.128 second long, with a sampling time of 8 ns
319 and the pulse amplitude selected to be consistent with the output of a typical
320 fission chamber measurement chain (3% of the ± 16 V range were used). For

Data processing



Measurement

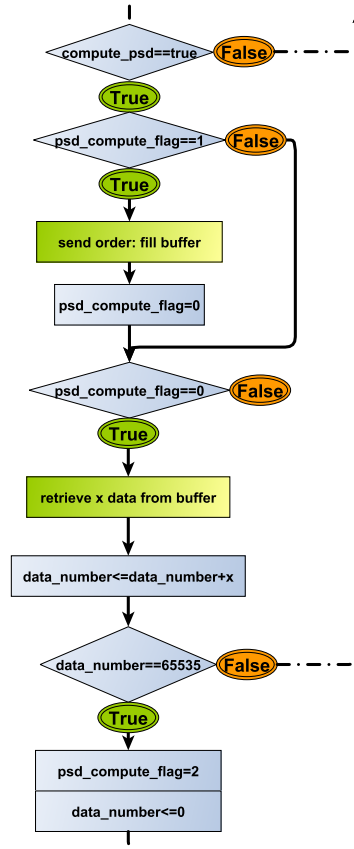


Figure 7: The control software dedicated to the smart detector module. (Only the measurement thread communicates with the FPGA smart detector module, even if the request for a new measurement is sent through the shared variable `psd_compute_flag` by the data processing thread.)

321 each pulse train, the third order cumulant estimator was computed before
 322 uploading to the signal generator and compared with the estimation of the
 323 measurement system. The results are summarized in the Table 1.

324 The measured third order cumulants are close to the computed ones. A
 325 maximum of 3.5 % of relative overestimation was found during these tests.
 326 The discrepancy is most probably due to the electronics transfer function and
 327 the truncation made by the ADC. Investigations has shown that the trans-
 328 fer function results a slight reshaping, therefore the measured estimation is
 329 slightly higher then the computed cumulant. Nevertheless, in practical sit-
 330 uations the calibration methodology will inherently take into account the
 331 reshaping, hence the count rate will not be overestimated.

c. rate (c/s)	$k3$ (computed)	$k3_a$ (measurement)	$k3_b$ (measurement) μs
$4 \cdot 10^6$	$2.84 \cdot 10^{-5}$	$(2.90 \pm 0.01) \cdot 10^{-5}$	$(2.91 \pm 0.19) \cdot 10^{-5}$
$4 \cdot 10^7$	$5.70 \cdot 10^{-5}$	$(5.85 \pm 0.02) \cdot 10^{-5}$	$(5.86 \pm 0.36) \cdot 10^{-5}$
$4 \cdot 10^6$	$3.22 \cdot 10^{-5}$	$(3.33 \pm 0.02) \cdot 10^{-5}$	$(3.37 \pm 0.27) \cdot 10^{-5}$
$4 \cdot 10^5$	$1.15 \cdot 10^{-5}$	$(1.19 \pm 0.02) \cdot 10^{-5}$	$(1.27 \pm 0.27) \cdot 10^{-5}$

Table 1: Computed and measured third order estimators for pulse trains at various count rates. $k3_a$ refers to the estimation based on 34 ms samples and $k3_b$ refers to the estimation based on 262 μs samples.

332 4.1.2. Smart detector module validation

333 In order to test the smart detector module, and the PSD measurement
 334 capabilities of the system, several pulse trains with a length of 0.128 s were
 335 simulated, and played with the signal generator. The trains contained Gaus-
 336 sian shaped pulses with a mean count rate of 10^6 c/s. The width (i.e. the
 337 standard deviation of the Gaussian) of the pulses were changed (5 ns, 10 ns
 338 and 15 ns were considered).

339 The obtained power spectral densities are available in Fig.8. As it can
 340 be seen, the spectrum shape is characteristic of the pulse shape. The line
 341 centered around 1 MHz and its harmonics are artifacts due to the fact the
 342 same 0.128 s signal was played periodically. The functioning of the smart
 343 detector module was appropriate.

344 4.2. In reactor validation

345 Finally, the measurement device was tested during an experimental cam-
 346 paign at the Minerve facility of CEA [11].

347 Several setups were realized in order to assess the compatibility of the
 348 device with the standard nuclear instrumentation. During the campaign,

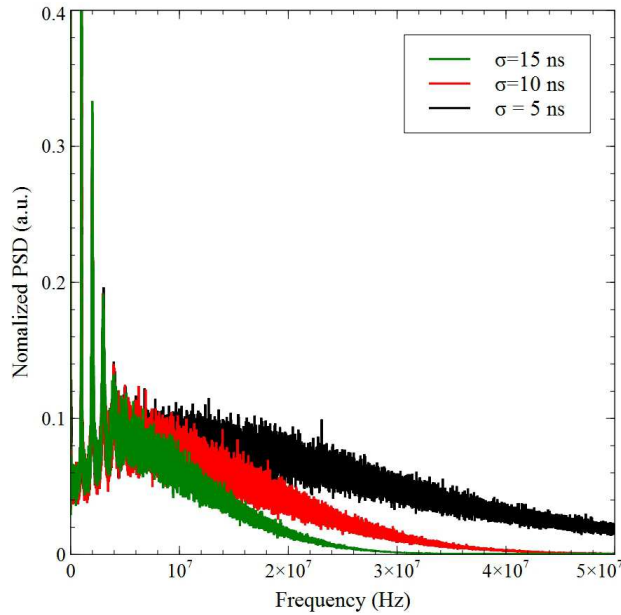


Figure 8: PSD obtained with simulated pulse trains.

349 two pre-amplifiers were used: the ADS, manufactured by Canberra and
 350 the PADF designed by the CEA instrumentation and electronics labora-
 351 tory. These pre-amplifiers are different in their output voltage and transfer
 352 function.

353 In order to cover a wide count rate range, two type of fission chambers
 354 were tested during the experiments: the CFUL01 (a relatively large chamber,
 355 which contains 1g of U235; its pulse shape is around 80 ns wide) and the
 356 CFUR (a rather small chamber, which contains 10 μ g of U235; its pulse shape
 357 is around 20 ns wide). At the same neutron flux, the CFUR chamber results
 358 5 orders of magnitude lower count rate than the CFUL01.

359 The CFUL01 chamber was located in the surrounding of the driver zone,
 360 whereas the CFUR was installed in the center of the reactor.

361 During the campaign, the following experiments were performed in order
 362 to assess various aspects of the measurement device:

- 363 • Cumulant estimation with the CFUL01 and the PADF at various power
 364 levels: to assess the linearity of the measurement system.
- 365 • Cumulant estimation with the CFUR and the PADF at various power

- 366 levels: to assess the limits of the system at low count rates.
- 367 • Pulse train recording with the CFUR and the PADF at various power
368 levels: to calibrate the HOC system (in order to retrieve the count rate
369 with the higher order method), and to estimate the count rate with
370 pulse counting algorithms.
 - 371 • PSD measurement with the CFUL01 and the ADS pre-amplifier with
372 various bias voltages: to simulate a detector failure and to measure the
373 change of the spectral width.

374 4.2.1. Third order cumulant measurements, CFUL01/PADF

375 The third order cumulant has been estimated at reactor powers between
376 10 W and 80 W with the CFUL01, based on 33 ms time windows. Both the
377 ± 0.6 V and the ± 16 V input ranges have been used, in order to assess the
378 linearity with both ranges.

379 The signal saturates at 30 W reactor power, when measured with low
380 voltage range. Therefore, only two measurements were done with this range
381 (at 10 W and 20 W). The cumulant over power ratios are $(4.04 \pm 0.36) 10^6$
382 (a.u.) \cdot W $^{-1}$ and $(4.11 \pm 0.28) 10^6$ (a.u.) \cdot W $^{-1}$ for the 10 W and 20 W power,
383 respectively. Although, in the future a better resolution of the power is
384 needed to draw deeper conclusion, the good agreement of the ratios implies
385 that the behavior is linear.

386 With the ± 16 V range the whole power range was covered. The obtained
387 cumulant estimations are presented in Fig.9. The measured third order cumulant
388 shows linearity with the reactor power. The departure from linearity
389 is lower than 1.6 %, which is the result of the random error of the estimation.
390 In order to estimate the count rate, the measurement chain has to be
391 calibrated. The calibration, through applying the methodology described
392 in [12] (namely, to evaluate the coefficient C_n in Eq. (1) by measuring the
393 mean pulse and the pulse amplitude distribution at low power), was planned
394 to be done during the post-processing of recorded signal samples. Unfortunately,
395 for this purpose the signal was recorded with the high voltage range,
396 which was not appropriate to discriminate properly the single pulses from
397 the noise. In the future, when further reactor time can be obtained for similar
398 measurement purpose, the calibration is going to be repeated with the
399 low voltage range as well. In order to avoid similar problems, also a new
400 calibration procedure is under development, which can be performed during
401 the real-time operation, and does not require post-processing. Nevertheless,
402 the measurement with the CFUL01 was still valuable to assess the linear
403 cumulant estimation of the measurement device.

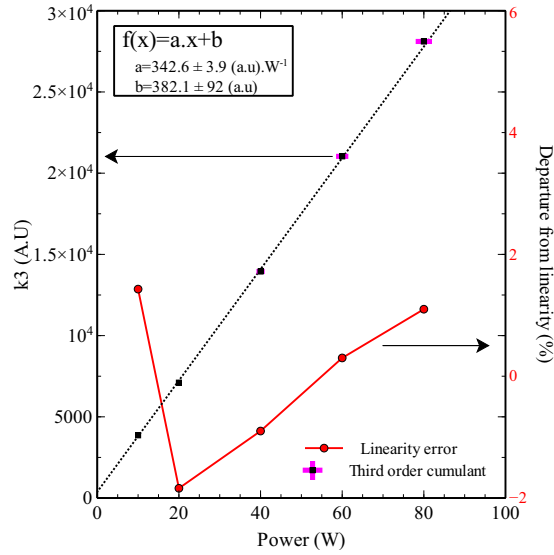


Figure 9: Third order cumulant recorded with the $\pm 16\text{V}$ range as a function of the reactor power.

4.2.2. Third order cumulant measurements, CFUR/PADF

Measurements with the CFUR chamber were performed only with the low voltage range, since the count rate of the signal was expected to be rather low on the power range of Minerve.

The measurements were done at 40 W and 80 W power level. The results are summarized in Table 2. The cumulant estimation based on one 33 ms long sample results a high standard deviation, which is expected since at these count rates only few pulses appear during one sample, and the number of observed pulses is uncertain. Nevertheless, the expected value of the cumulant estimator was based on 1900, 33 ms long signal samples, therefore the overall deviation of the estimated mean cumulant is less than 2.3%. (In comparison, when the reactor was all control rods down and estimation was based only on the noise in the system, the estimated third order cumulant appeared to be 350 ± 50 , which is less than the deviation of the cumulant estimation for the fission chamber signal). The mean cumulant over the power ratios show good agreement, which implies linear behaviour. For the estimated count rates (discussed later), the deviation refers to the $400 \cdot 0.52$ ms sample, not only to one sample.

To calibrate the fission chamber through the methodology presented

Table 2: Cumulant and count rate estimations with the HOC module and with pulse counting.

Power (W)	k_3 (a.u.)	$\langle k_3 \rangle / P$ (a.u.) $\cdot W^{-1}$	HOC count rate c/s	Ref. count rate c.s
40	$(1.18 \pm 0.39) 10^4$	295 ± 12	3430 ± 354	(2861 ± 118)
80	$(2.38 \pm 0.56) 10^4$	297 ± 10	6918 ± 686	(6103 ± 171)

423 in Ref. [12], the raw signal recorder module dedicated to smart detector
 424 was used, with a minimalist control software. Several signal segments were
 425 recorded at 80 W and the pulses were isolated during post-processing in or-
 426 der to determine the calibration coefficient in (1). From the measurements
 427 nearly 2700 pulses were isolated, which allows to have acceptable statistics.
 428 The mean pulse shape and the amplitude distribution of the pulses is illus-
 429 trated in Fig. 10. As one can see, the dynamic of the measurement system
 430 allows to discriminate the pulses from the noise and the resolution is fine
 431 enough to observe even the current bouncing back from the cable (a small
 432 bump following the main pulse). The prototype is capable of working as
 433 a raw signal recorder as well. The estimated calibration coefficient for the
 434 third order is:

$$C_{clas} = 3.44 \pm 0.3 \text{ (a.u.)} \cdot s/c \quad (5)$$

435 The calibration has large uncertainty, which shows the disadvantage of this
 436 methodology. As it was highlighted in Ref. [12] as well, for the high order
 437 methods an empirical calibration may be favorable. Such calibration is not
 438 plausible for the traditional Campbelling method, due to the linearity gap
 439 between pulse counting methods and the second order Campbelling.

440 In order to obtain a reference count rate, 400 signal segments recorded at
 441 a reactor power of 80W and 400 recorded at a power of 40 W were analyzed
 442 with pulse counting method as well. The estimated count rates obtained
 443 by pulse counting, and the ones computed from the calibrated higher order
 444 Campbelling are included in Table 2. It has to be highlighted again that
 445 the standard deviation refers to the $400 \cdot 0.52\text{ms}$ long signal sample for the
 446 counting algorithm result while it is related to the $1900 \cdot 33 \text{ ms}$ long signal for
 447 the calibrated HOC. The standard deviation of an estimation based on one
 448 0.52 ms sample is much higher for the pulse count, but the goal was to define
 449 the reference (i.e. the real) count rate of the chamber at these powers. The
 450 good agreement of the estimated count rates show that the results measured

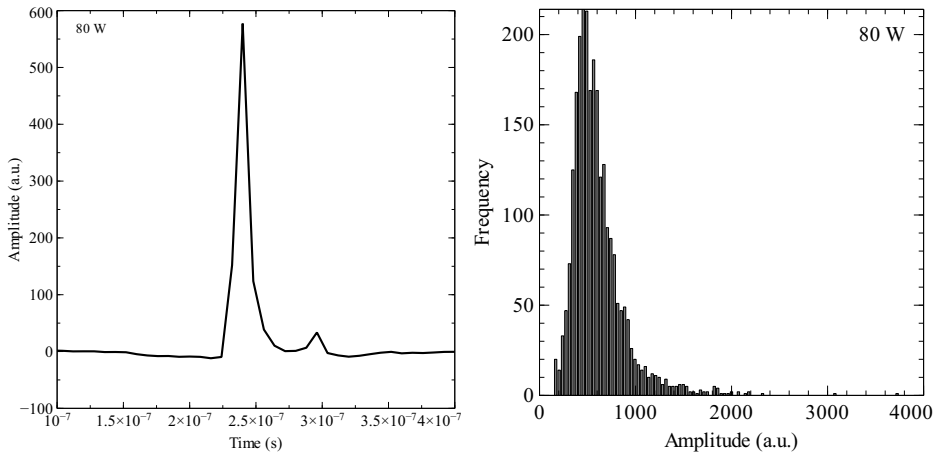


Figure 10: Left: mean pulse shape computed with single pulses coming from the 80 W measurement data. Right: amplitude distribution of pulses computed on datasets recorded at 80 W.

451 by the system are physically correct. The results also imply that monitoring
 452 at really low count rates (in the order of 10^3 cps) is possible with higher order
 453 Campbelling, but longer measurements are necessary (nevertheless, the same
 454 holds for pulse mode measurements as well).

455 4.2.3. PSD measurements, CFUL01/ADS

456 When the tests of the smart detector module were performed, only the
 457 ADS preamplifier were available, which allowed to verify that the device is
 458 capable to work with other instruments as well.

459 The ADS pre-amplifier and a CFUL01 chamber were used to test the
 460 smart detector module. Using the CFUL01 was advantageous for this pur-
 461 pose, since it has a higher count rate, therefore its power spectral density
 462 can be measured more accurately during real time operation.

463 In the current experimental work, the change of the pulse shape was
 464 achieved by changing the fission chamber voltage in the saturation regime.
 465 The increase of the voltage has similar effects on the pulse width as the
 466 decrease of the gas pressure, but it is simpler to achieve during the measure-
 467 ment.

468 Measurements were taken at a constant reactor power of 20 W with the
 469 voltage changed between 600 V and 850 V. For each applied voltage, the PSD
 470 was constructed by using 4000 datasets of 0.52 ms long signals. The low vari-

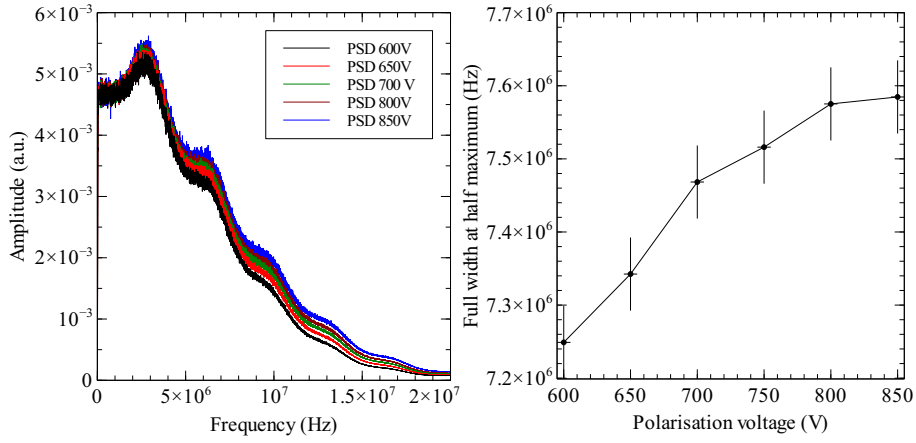


Figure 11: Left: PSD as a function of the applied voltage. Right: Spectral width as a function of the polarisation voltage.

471 ance of the spectra estimated from this amount of data, allows to distinguish
 472 change in the spectral as small as 50 kHz. The measured PSD and the esti-
 473 mated spectral width are presented in Fig.11. The slight oscillation of the
 474 PSD is an artifact due to the applied cable. As expected, the spectral width
 475 increases with the increase of the applied voltage, and it saturates at high
 476 voltages. The reason of the saturation of the spectral width is the saturation
 477 of electron drift velocity in argon-nitrogen mixtures at high reduced electric
 478 fields [13].

479 Therefore, the proof of concept of the smart detector is validated: it
 480 is possible to detect a change of mean pulse shape from investigating the
 481 power spectral density, whereas the measurement noise and the low frequency
 482 filtering of the system have negligible influence on the determination of the
 483 spectral width.

484 Although, in the current experiment, the time needed to record and pro-
 485 cess the 4000 datasets is approximately 300 s due to the slow data transfer,
 486 this already allows to test in every 5 minutes whether the chamber malfunc-
 487 tions. However, the processing time of the smart detector prototype could
 488 be reduced by a factor of 3 by using optimised FFT routines, and in the
 489 future even faster tests can be achieved for the industrial application by
 490 implementing the same method on board with higher performance.

491 **5. Conclusion**

492 An innovative measurement system prototype for real time neutron mon-
493 itoring was presented and validated through this paper. The prototype was
494 built using an open source CPU/FPGA device with ADC on board. Such
495 architecture has a several advantages: time critical, simple operations can
496 be performed on the FPGA, immediately after recording the data, whereas
497 complex and heavy data processing can be performed on the CPU. The sim-
498 plicity of the chosen board (Red-Pitaya) allowed fast and straightforward
499 development.

500 The main purpose was to prove the feasibility of a real time neutron
501 flux monitoring system using the third order Campbell mode. This method
502 suppresses the impact of noise and provides wide range of operation. In this
503 work it was shown that the method is even capable to work at count rates
504 as low as 10^3 cps.

505 In the work, the concept of fission chamber failure detection was also
506 included. The self monitoring capability of the system is based on detected
507 the change in the width of the power spectral density of the signal.

508 The paper provides detailed description of the implemented FPGA al-
509 gorithms and the control software running on the CPU. All the challenges
510 and solutions were highlighted in order to serve as a tutorial for similar
511 developments.

512 The reliability of the concepts and the robustness of the device was tested
513 through an experimental campaign at the Minerve reactor. The linear re-
514 sponse and the real time operation of the device was verified over a wide
515 power range. Through the calibration of the system the physical validity of
516 the measured results was assessed. The self monitoring capability was also
517 tested, the system is capable to detect the change in the voltage set between
518 the electrodes of the chamber.

519 Since the calibration of the system is rather elaborate, a simpler, auto-
520 matic and real time calibration procedure is under development.

521 For industrial usage, the next step is going to be the implementation
522 of the same concepts on a board which has higher performance in order to
523 achieve faster self monitoring capability.

524 **Acknowledgment**

525 This study was partly supported by the CEA INSNU and TECNA Projects
526 and by the Swedish Research Council (Grant No.B0774801). This study also

527 part of an on-going collaboration project on the instrumentation and safety
528 of sodium cooled fast reactors between Chalmers and CEA.

- 529 [1] C. Jammes, N. Chapoutier, P. Filliatre, J. P. Jeannot, F. Jadot, D. Ver-
530 rier, A.-C. Scholer, B. Bernardin, Neutron flux monitoring system of
531 the French GEN-IV SFR: Assessment of diverse solutions for in-vessel
532 detector installation, *Nuclear Engineering and Design* 270 (2014) 272–
533 282.
- 534 [2] C. Jammes, P. Filliatre, B. Geslot, T. Domenech, S. Normand, Assess-
535 ment of the high temperature fission chamber technology for the french
536 fast reactor program, *IEEE Transactions on Nuclear Science* 59 (2012)
537 1351–1359.
- 538 [3] N. R. Campbell, V. J. Francis, A theory of valve and circuit noise,
539 *Journal of the Institution of Electrical Engineers-Part III: Radio and*
540 *Communication Engineering*.
- 541 [4] I. Lux, A. Baranyai, Higher order campbell techniques for neutron flux
542 measurement, *Nuclear Instruments and Methods in Physics Research*
543 202.
- 544 [5] L. Pál, I. Pázsit, Zs. Elter, Comments on the stochastic characteristics
545 of fission chamber signals, *Nuclear Instruments and Methods in Physics*
546 *Research Section A: Accelerators, Spectrometers, Detectors and Asso-*
547 *ciated Equipment* 763 (2014) 44–52.
- 548 [6] E. Parzen, *Stochastic Processes, Classics in Applied Mathematics*, 1999.
- 549 [7] Zs. Elter, M. Bakkali, C. Jammes, I. Pázsit, Performance of Higher
550 Order Campbell methods, Part I: review and numerical convergence
551 study, *Nuclear Instruments and Methods in Physics Research Section*
552 *A: Accelerators, Spectrometers, Detectors and Associated Equipment*
553 821 (2016) 66 – 72. doi:<http://dx.doi.org/10.1016/j.nima.2016.03.023>.
- 554 [8] Zs. Elter, P. Filliatre, G. de Izarra, I. Pázsit, C. Jammes, Self-monitoring
555 fission chamber: theoretical groundwork, in: *Physor conference*, 2016.
- 556 [9] M. Galassi, J. Davies, J. Theiler, B. Gough, al., *GNU Scientific Library*
557 *Reference Manual* (3rd Ed.).
- 558 [10] Xilinx, *7 Series FPGAs Memory Resources*, 2014.

- 559 [11] G. Bignan, P. Fougeras, P. Blaise, J.-P. Hudelot, F. Mellier, Reactor
560 physics experiments on zero power reactors, in: D. Cacuci (Ed.), Hand-
561 book of Nuclear Engineering, Springer US, 2010, pp. 2053–2184.
- 562 [12] Zs. Elter, G. de Izarra, P. F. C. Jammes, I. Pázsit, Performance of Higher
563 Order Campbell methods, Part II: calibration and experimental appli-
564 cation, Nuclear Instruments & Methods in Physics Research, Section A:
565 Accelerators, Spectrometers, Detectors, and Associated Equipment Been
566 submitted.
- 567 [13] G. Haddad, Drift velocity of electrons in nitrogen-argon mixtures, Aust.
568 J. Phys. 36 (1983) 297–303.